

Location Performance and Detection Threshold of the Spanish National Seismic Network

ANTONINO D’ALESSANDRO,¹ JOSÉ BADAL,² GIUSEPPE D’ANNA,¹ DIMITRIS PAPANASTASSIOU,³
IOANNIS BASKOUTAS,³ and NURCAN M. ÖZEL⁴

Abstract—Spain is a low-to-moderate seismicity area with relatively low seismic hazard. However, several strong shallow earthquakes have shaken the country causing casualties and extensive damage. Regional seismicity is monitored and surveyed by means of the Spanish National Seismic Network, maintenance and control of which are entrusted to the Instituto Geográfico Nacional. This array currently comprises 120 seismic stations distributed throughout Spanish territory (mainland and islands). Basically, we are interested in checking the noise conditions, reliability, and seismic detection capability of the Spanish network by analyzing the background noise level affecting the array stations, errors in hypocentral location, and detection threshold, which provides knowledge about network performance. It also enables testing of the suitability of the velocity model used in the routine process of earthquake location. To perform this study we use a method that relies on P and S wave travel times, which are computed by simulation of seismic rays from virtual seismic sources placed at the nodes of a regular grid covering the study area. Given the characteristics of the seismicity of Spain, we drew maps for M_L magnitudes 2.0, 2.5, and 3.0, at a focal depth of 10 km and a confidence level 95 %. The results relate to the number of stations involved in the hypocentral location process, how these stations are distributed spatially, and the uncertainties of focal data (errors in origin time, longitude, latitude, and depth). To assess the extent to which principal seismogenic areas are well monitored by the network, we estimated the average error in the location of a seismic source from the semiaxes of the ellipsoid of confidence by calculating the radius of the equivalent sphere. Finally, the detection threshold was determined as the magnitude of the smallest seismic event detected at least by four stations. The northwest of the peninsula, the Pyrenees, especially the westernmost segment, the Betic Cordillera, and Tenerife Island are the best-monitored zones. Origin time and focal depth are data that are far from being constrained by regional events. The two Iberian areas with moderate seismicity and the highest seismic hazard, the Pyrenees and Betic Cordillera, and the northwestern quadrant of the peninsula, are the

areas wherein the focus of an earthquake is determined with an approximate error of 3 km. For M_L 2.5 and M_L 3.0 this error is common for almost the whole peninsula and the Canary Islands. In general, errors in epicenter latitude and longitude are small for near-surface earthquakes, increasing gradually as the depth increases, but remaining close to 5 km even at a depth of 60 km. The hypocentral depth seems to be well constrained to a depth of 40 km beneath the zones with the highest density of stations, with an error of less than 5 km. The M_L magnitude detection threshold of the network is approximately 2.0 for most of Spain and still less, almost 1.0, for the western sector of the Pyrenean region and the Canary Islands.

Key words: Ambient noise, P and S travel times, power spectral density, errors in hypocentral location, detection threshold, Spanish national seismic network.

1. Introduction

Seismic networks are useful for monitoring seismically active regions and are, consequently, a powerful tool for monitoring earthquake occurrence and the tectonic processes affecting the monitored area. Their applications are numerous: surveillance of seismogenic zones, early warning systems, seismic hazard and seismic risk studies, etc. An appropriately configured seismic network is also a valuable tool for study of near-surface seismic velocity structures (BADAL *et al.*, 2004), large and deep geological domains (CHEN *et al.*, 2010), using respectively short and long-wavelength seismic tomography, and site effects, etc. The capability of accurately detecting small-to-intermediate earthquakes requires a seismic network with a sufficient number of optimally distributed low-noise stations. In this context it is important to assess the capability of the existing array to identify those seismogenic areas that might not to be adequately monitored by the network, and to determine, from a strictly quantitative perspective, the error margins of focal data estimates.

¹ Istituto Nazionale di Geofisica e Vulcanologia, Centro Nazionale Terremoti, Roma, Italy. E-mail: antonino.dalessandro@ingv.it

² Physics of the Earth, University of Zaragoza, Pedro Cerbuna 12, 50009 Zaragoza, Spain.

³ Institute of Geodynamics, National Observatory of Athens, Athens, Greece.

⁴ Kandilli Observatory and Earthquake Research Institute of Istanbul, Istanbul, Turkey.

Other aspects, for example enlargement and improvement of the tested network to achieve more precise and reliable detection of seismic events, are issues that can be tackled later. The purpose of the work discussed in this paper was to evaluate the performance of the Spanish National Seismic Network (SNSN) which monitors the seismicity of the Spanish territory (MÉZCUA, 1995) and is operated by the Instituto Geográfico Nacional (IGN). The IGN is currently one of the three hubs of the Euro-Mediterranean Seismological Centre, and 120 seismic stations are distributed throughout its national territory (Table 1). More details can be found on the IGN website (<http://www.ign.es>).

Spain is located in the westernmost segment of the Eurasia–Africa plate boundary, forming a sub-continental domain in the framework of a tectonically complex area subjected to strong stresses distributed over a wide area (BUFORN and UDÍAS, 2010). Spain has low-to-moderate seismicity (SAMARDJIEVA and BADAL 1999; LÓPEZ CASADO *et al.*, 2000) and similar seismic hazard (PELÁEZ MONTILLA and LÓPEZ CASADO 2002). Most of the epicenters of Iberian earthquakes are concentrated in the south and southeast of Spain and in the Pyrenees (Fig. 1a) (BADAL *et al.*, 2005a). The seismicity along the Betic Cordillera is associated with continent–continent collision between the African and Eurasian plates whereas the seismic activity in the Pyrenean zone is because of the differential rotation of the peninsula, which is able to uplift this mountain range (Fig. 1b). In both cases the seismic energy is predominantly released by shallow and frequent events of small magnitude. After revising M_s magnitudes from 3.0 to 9.0 and focal depths down to 200 km from NEIC data, the results show that almost all earthquakes are shallow events with focal depth constrained between 0 and 30 km, because only 5.06 % of the earthquakes are deeper and almost all of them have M_s magnitude ≤ 4.9 , because only 1.51 % have magnitude between 5.0 and 6.9 (BADAL *et al.*, 2005b).

BADAL *et al.* (2000) studied moment magnitudes for early (1923–1961) instrumental Iberian earthquakes and counted only 18 earthquakes with focal depths from 6 to 30 km, which were felt in the Iberian Peninsula with epicentral intensity equal to or larger than VI MSK. Actually, only two events had

epicentral intensity VI; the rest had intensities VII or VIII MSK. Among these events is the 19 April 1956 Albolote (southern Spain) earthquake, m_b 5.0, M_s 5.4, approximate depth 8 km, epicentral intensity VII–VIII MSK, that caused serious damage and 11 deaths (including four by landslide). From the registered historical earthquake data we have news of only two really destructive Iberian earthquakes that occurred in the nineteenth century. The first was the 21 March 1829 Torrevieja (southeast of Spain) earthquake, m_b 6.3 ± 0.4 , M_s 6.9 ± 0.6 , approximate depth 10 km (LÓPEZ CASADO *et al.*, 2000). This big shock, with maximum intensity X MSK (MUÑOZ and UDÍAS, 1987), caused widespread damage and approximately 1,000 deaths and 1,500 injured individuals (RODRÍGUEZ DE LA TORRE, 1984). The second was the 25 December 1884 Arenas del Rey (south Spain) earthquake, with epicenter between Málaga and Granada, M_L 6.5, m_b 6.1 ± 0.4 , M_s 6.5 ± 0.6 , and depth 10–20 km (LÓPEZ CASADO *et al.*, 2000). This quake, which probably reached maximum MSK intensity X (MUÑOZ and UDÍAS, 1987), completely destroyed several small villages and damaged 13,000–14,000 buildings (4,400 were wholly demolished), and caused approximately 800 deaths and 1,500 injured individuals (UDÍAS, 1999). Macroseismic MSK intensities VIII and IX MSK for a return period of 100 and 500 years, respectively, are expected in the area (PAYO *et al.*, 1994). That said, we must stress here the recent quake that occurred on 11 May 2011 at Lorca (southeastern Spain), which despite its moderate magnitude (M_s 5.1) was a destructive, very shallow earthquake (~ 2 km) that caused nine deaths and destroyed a large number of buildings.

According to the Global Seismic Hazard Map (SHEDLOK *et al.*, 2000) showing peak ground acceleration (pga) with a 10 % chance of exceedance in 50 years, the seismic hazard of the Iberian Peninsula is 0.04–0.16 g units. The European–Mediterranean Seismic Hazard Map (JIMÉNEZ *et al.*, 2001), also calculated for pga with a 10 % probability of exceedance in 50 years (475 year return period), confirms this value. Examining the seismic hazard map of Spain for a 500 year return period as standard (BOE, 2002) to ensure the resistance of any man-made structure before the possibility of an earthquake, pga values

Table 1

Code, location, and altitude of stations belonging to the Spanish National Seismic Network under the control of the Instituto Geográfico Nacional

Code	Lat.	Long.	Alt.	Code	Lat.	Long.	Alt.
ACU	38.5113	-0.4107	580	EMLI	35.3000	-2.9500	0
AFON	38.6649	-0.5412	1120	EMON	43.4362	-7.3298	615
ATE	43.0858	-0.7003	0	EMOS	40.3639	-0.4721	1694
CCAN	28.2216	-16.6050	2210	EMUR	37.8422	-1.2405	574
CFON	41.7623	2.4356	973	ENIJ	36.9715	-2.2070	440
CFTV	28.4138	-14.0833	540	EORO	42.8926	-1.3095	880
CHIE	27.7270	-17.9607	170	EOSO	28.0718	-15.5525	760
CHIO	28.2398	-16.8162	432	EPAB	39.5449	-4.3499	946
CICO	28.3490	-16.7241	785	EPLA	40.0642	-6.0803	591
CLAN	29.1028	-13.4761	868	EPOB	41.3527	1.0786	890
CLLI	42.4792	1.9742	1413	EPON	43.3270	-7.1494	440
CSOR	42.3756	1.1339	1227	EPRU	36.9660	-5.2313	560
CTFE	28.4800	-16.2620	270	EQES	37.8028	-3.0711	1140
CTIG	27.7882	-17.9221	530	EQTA	37.2050	-3.4399	1100
EADA	38.1673	-4.5771	565	EQUE	37.2086	-3.4444	1050
EAGO	42.8027	-8.0892	500	ERIP	37.3730	-7.2550	82
EAJ	28.5399	-16.3434	239	ERON	37.0180	-3.8050	1305
EALB	35.9399	-3.0343	20	EROQ	40.8232	0.4088	284
EALH	37.8582	-1.4197	294	ERTA	40.9567	0.3335	547
EALK	43.2197	-1.5071	965	ERUA	42.3927	-7.1425	431
EARA	42.7727	-1.5797	476	ESAC	41.7219	-0.4693	815
EARI	43.3012	-5.2099	680	ESEL	39.7682	2.8943	231
EBAD	38.7556	-7.0133	221	ESPR	36.8686	-5.8562	135
EBAN	38.1710	-3.7900	460	ETER	42.3015	2.8555	238
EBEN	38.7038	-0.2250	764	ETOB	38.6447	-1.5478	855
EBER	36.8979	-2.8896	1690	ETOR	40.8195	-2.0552	1018
EBIE	42.6862	0.1428	2130	ETOS	39.7678	2.8144	480
EBR	40.8205	0.4933	0	EVAL	37.5842	-6.7475	295
ECAB	38.0753	-5.4186	520	EVIA	38.6386	-2.5025	1142
ECAL	41.9413	-6.7371	950	EZAM	42.1490	-8.6950	398
ECEU	35.8978	-5.3768	278	GGC	28.1197	-15.6367	560
ECHÉ	39.5908	-0.9677	643	GORA	37.4793	-3.0417	868
ECOG	37.2772	-3.5663	1176	GUD	40.6430	-4.1537	1268
ECRI	42.6089	-2.5100	807	IELO	42.8432	-1.2366	819
EFAM	29.1275	-13.5295	135	IEPA	42.7794	-1.2669	769
EGOM	28.1594	-17.2096	782	IPRE	42.8047	-1.3569	531
EGRA	42.1952	0.3160	706	IUNC	42.7559	-1.4989	766
EGRO	37.5342	-7.4831	130	IUSE	42.9469	-1.5478	870
EGUA	36.8337	-3.5653	386	IZUN	42.8610	-1.4564	701
EHIG	28.5567	-17.8062	845	MACI	28.2502	-16.5082	1591
EHOR	37.8232	-5.2480	160	MELI	35.2899	-2.9392	60
EHRO	27.7535	-18.1106	135	MVO	41.1643	-7.0288	55
EHUE	37.8148	-2.5927	980	OKGL	36.0370	0.6561	594
EIBI	39.0269	1.3436	260	PAB	39.5458	-4.3483	925
EINC	42.6600	-7.3500	739	PFVI	37.1328	-8.8268	0
EJIF	36.4513	-5.4688	260	PMAFR	38.9553	-9.2827	329
EJIM	36.4358	-5.4542	203	PMOZ	32.8230	-17.1970	1027
EJON	42.4487	2.8886	570	RETOR	40.8192	-2.0552	1018
ELAN	43.2317	-3.4340	633	ROSA	38.7208	-28.2470	31
ELIJ	36.9190	-5.3790	870	SELV	37.2362	-3.7285	65
ELIZ	43.1640	-1.5285	523	SESP	38.1197	-2.5464	1528
ELOB	41.8674	-8.0611	980	SJAF	42.4845	2.8822	0
ELOJ	37.1480	-4.1530	998	STS	42.8860	-8.5509	265
ELUQ	37.5605	-4.2668	703	TBT	28.6794	-17.9145	180

Table 1 continued

Code	Lat.	Long.	Alt.	Code	Lat.	Long.	Alt.
EMAL	36.7620	-4.4280	131	YARA	42.6477	-1.1902	1303
EMAZ	42.9490	-8.9765	405	YASP	42.7292	-1.1634	692
EMEL	35.3000	-2.9567	85	YBER	42.5810	-0.9182	632
EMIJ	36.5645	-4.7727	470	YNAR	42.6375	-1.3672	740
EMIN	37.7675	-6.6724	240	YSOS	42.4554	-1.1470	881
EMIR	41.9144	1.5258	841	YUND	42.5768	-1.1331	872

from 0.12 to 0.16 g can be expected at some places in the Pyrenees, and horizontal ground acceleration up to 0.24 g (2.4 m/s²) can be expected around Granada zone and other sites along the south-southeast zone of the peninsula near the Mediterranean coastline (Fig. 1c).

The SNSN is configured with the purpose of monitoring, as well as possible, those areas of the Iberian Peninsula with the greatest concentration of earthquake epicenters. With this purpose the seismic stations in the array were mainly placed over the south-southeast flank and the Pyrenean band to north of the peninsula (Fig. 1d). In the work discussed in this paper we studied the noise conditions, reliability, and seismic detection capability of the SNSN by analysis of the background noise level recorded by the network stations, errors in hypocentral location, and detection threshold, which provided us updated information about the current potential of the Spanish network. We began by assessing the background noise from the power spectral density computed from the vertical ground acceleration in the 1–12 Hz frequency range, thus discriminating areas with different noise level. We then determined *P* and *S* residual times and the variation of the *P*/*S* ratio between residual times as a function of the hypocentral distance. These tests enable a first assessment of the suitability of the velocity model used by the IGN for earthquake location. Mean values of *P* and *S* residual times and their respective variances versus hypocentral distance were also calculated to check both the deviation from the optimum estimator (bias) and the stability of the estimator (variance) relative to the observed data. The mathematical support we used to perform this study consisted of *P* and *S* wave travel times obtained by simulating seismic waves propagating from virtual seismic sources (D'Alessandro *et al.*, 2011a).

Last, it is important to stress that we were interested in dealing strictly with the performance of the Spanish network starting from its current geometrical configuration and the velocity model used for event location; other issues concerning purely technical aspects of the network itself, for example seismic instruments installed, data transmission systems, event-detection algorithm, ray-tracer, early warning time, etc., are beyond the scope of this article.

2. Method

The methods so far proposed to evaluate the performance of a seismic network are mainly based on the estimation of the magnitude of completeness M_C , i.e., the lowest magnitude at which all earthquakes in a space-time volume are reliably detected (RYDELEK and SACKS, 1989; SERENO and BRATT, 1989; GOMBERG, 1991; WIEMER and WYSS, 2000; MARSAN, 2003; WOESSNER and WIEMER, 2005; AMORÈSE, 2007; SCHORLEMMER and WOESSNER, 2008). As is well known, M_C is a function of the time period investigated and may vary substantially because of spatial and temporal variations of seismicity and network geometry. For the Spanish network, for example, the magnitudes of completeness reported by PELÁEZ MONTILLA and LÓPEZ CASADO (2002) are 2.5, 3.5, 4.5 and 5.5 for seismicity since 1960, 1929, 1700, and 1300, respectively. It is common practice to obtain the completeness magnitude by investigating the earthquake catalog by use of different methods, namely: from the hypothesis of self-similarity and changes of the network between day and night (RYDELEK and SACKS, 1989), by comparing amplitude-distance curves with the signal-to-noise ratio (SERENO and BRATT, 1989), from amplitude thresholds (GOMBERG, 1991), and by assessing the quality of the

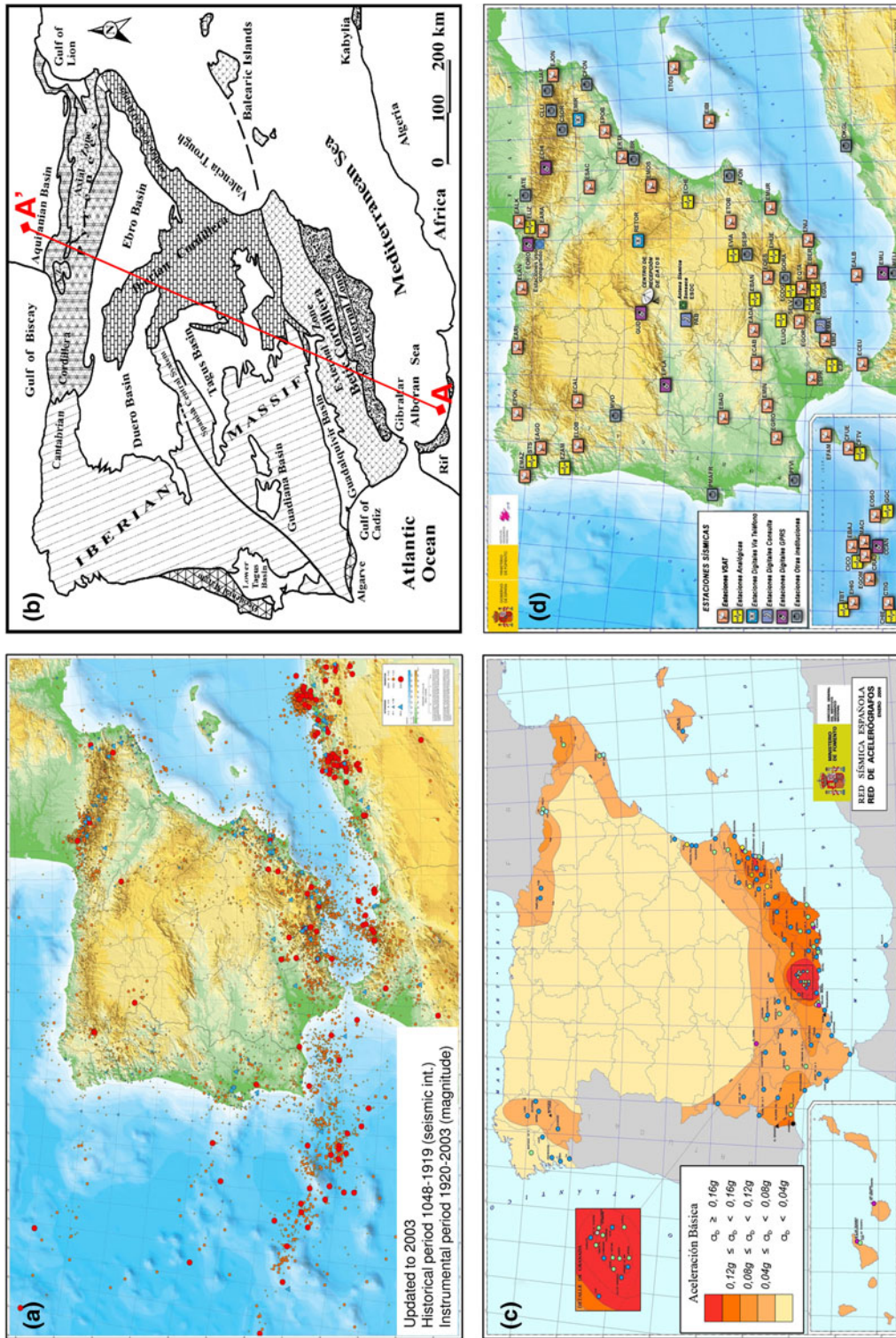


Figure 1
a Geographical distribution of earthquake epicenters (*circles*) in the Iberian Peninsula and adjacent areas updated to 2003 (map at scale 1:2,250,000; source: IGN). **b** Main tectonic units in the Iberian Peninsula (HENARES *et al.*, 2010). The transect AA' (35.41°N, -4.64°E; 43.94°N, -0.8°E) in the north-south direction marks the position of a vertical section which is presented later (Fig. 9). **c** Official seismic hazard map of Spain based on horizontal ground surface acceleration (in g units), used for the antisismic design of buildings and other structures under the NCSR-02 standard (map at scale 1:4,000,000; source: IGN). **d** Location of SNSN stations (source: IGN)

earthquake catalog (WOESSNER and WIEMER, 2005). Statistical methods are also used, for example the entire-magnitude-range (EMR) method (OGATA, 1993), the goodness-of-fit test (GFT) (WIEMER and WYSS, 2000), the maximum curvature method (MAXC) (WIEMER and WYSS, 2000), *b*-value stability (MBS) (CAO and GAO, 2002), optimized seismic threshold monitoring (KVAERNA *et al.*, 2002), the change-point detection method on frequency-magnitude distributions (AMORÈSE, 2007), the probability of detecting an earthquake at each seismic station (SCHORLEMMER and WOESSNER, 2008), and Bayesian estimation (MIGNAN *et al.*, 2011).

M_C is itself an important variable when testing the completeness of earthquake catalogs and for most studies related to seismicity, but it really does not give any information about the spatial distribution of possible errors in hypocentral location. These errors are a function of the accuracy of the velocity model used for this purpose, but also of the geometry and density of the array and, of course, of the noise affecting the stations that make up the network. For this reason we use a new method of analysis called seismic network evaluation through simulation (SNES; D'ALESSANDRO *et al.*, 2011a, b, 2012a, b, c) to evaluate the location performance and detection threshold or capability of the SNSN. The SNES method needs for its implementation (as inputs): the location of all network stations, the environmental noise that affects them, a seismic velocity model for hypocentral location, and empirical laws to estimate the variance of residual travel times. In addition, to provide information on the natural noise affecting the seismic network and the adequacy of the velocity model involved in the operations, the SNES method, depending on the earthquake magnitude, also gives:

1. the set of stations involved in the earthquake location process and their respective azimuthal gaps, which enables identification of those stations that are useful for earthquake location and in some way assessing the reliability of the epicenter solution;
2. confidence intervals of the hypocentral determinations given the geometry and natural noise affecting the array stations; and

3. the detection threshold of the seismic network under verification checking.

From an analytical perspective, the SNES method can be systematized as follows:

1. Computation of power spectral density on the vertical component of the noise at each network station.
2. Determination of *P* and *S* residual travel times versus hypocentral distance and empirical laws constraining the respective variances.
3. Computation of power spectral density curves of ground acceleration taking into account propagation effects.
4. Simulation of seismic rays coming from virtual seismic sources placed at the nodes of a regular grid that covers the study area.
5. Calculation of the ratio between the power spectrum of the synthetic signal and the power spectrum of the noise.
6. Estimation of the values of the hypocentral variables by inverse modeling and their uncertainties from the covariance matrix.
7. Estimation of the detection threshold as the magnitude of the smallest event detected by a prefixed number of stations.

More details about the SNES method, computation algorithms, and the results from its application to an important seismic network can be found in D'ALESSANDRO *et al.* (2011a, b, 2012a, b, c). In the work discussed in this paper we applied the SNES method to the SNSN to estimate background noise levels, to assess the suitability of the velocity model used in the location routine, to quantify uncertainties in hypocentral location, and to determine the detection threshold offered by the SNSN settings.

3. Environmental Noise Power

Background noise levels seriously affect the performance of a seismic network at the sites where the stations are installed. Obviously, the correct reading of the correlated seismic phases is highly dependent on the environmental noise level and the quality of the signal in the typical frequency range of regional

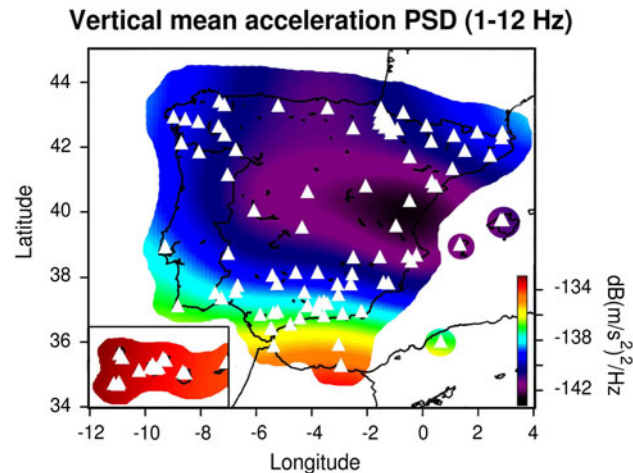


Figure 2

Ambient noise map based on power spectral density (PSD) in the 1–12 Hz frequency range, computed from vertical acceleration recorded by the Spanish array (*triangles*). Inverse distance weighting was used for standardization of grid data

events, or, more precisely, on the wideband spectral ratio (WSR). The accurate picking of Pg and Pn phases to partly control the reading errors requires WSR above 10. ZEILER and VELASCO (2009) have empirically verified that this type of error is approximately 0.1 s for WSR >10 and somewhat larger below this threshold.

The noise level affecting a seismic station is commonly investigated by using the power spectral density (PSD) of the noise record. Leaving aside the characteristics of the recording instrument, given that in this context the quality of the “signal” depends, especially, on the intrinsic noise level at the site, we estimated PSD from the vertical acceleration component of the ambient noise within the 1–12 Hz frequency range by use of PQLX software (McNAMARA and BULAND, 2004). The environmental noise level at SNSN stations was mapped by applying a two-dimensional (2D) interpolation function for irregularly-spaced data, e.g., the method of weighted inverse distance (SHEPARD, 1968; SERÓN *et al.*, 1999). Later, a 2D moving average was used for reduction of possible local effects related to faulty installations. Figure 2 shows the ambient noise power map for the SNSN. Undoubtedly, the noise levels reported on this map reveal trends, despite the fact that the results might reflect minimum, rather than average, values because of the smoothing procedure, or simply because the stations are normally placed on sites with

low noise. In any case these results may be of great help for people who manage the network, especially when choosing sites for installation of new seismic stations or when removing noisy stations. Thus, some areas, for example Andalusia (south Spain), northern Morocco, and the Canary Islands (inset in the bottom left corner) have relatively high noise levels whereas noise is low in the other regions, mostly distributed among the center, north, and east of the Iberian Peninsula, namely the Iberian Massif, Iberian Cordillera, Neogene Basins, Pyrenees, and Balearic Islands (Fig. 1b). The low noise of these sites corresponds with a lower density of seismic stations in these areas (Fig. 1d).

The high noise level of the stations in the Andalusian region and northern Morocco is probably related to the thick cover of sedimentary rocks in the Guadalquivir and Gharb basins, respectively. The Guadalquivir delta is filled with sand and marshland, and the Gharb basin with unconsolidated sediments and sand. The presence of weakly compacted sediments, where the seismic wave velocity is low, can give rise to resonance phenomena. These site effects, that are particularly strong and frequent in sedimentary basins and deltas, lead to ground motion amplification at the surface. The Canary archipelago comprises seven main islands of volcanic origin, of which three (Lanzarote, Tenerife, and La Palma) have had historical and recent seismic activity and

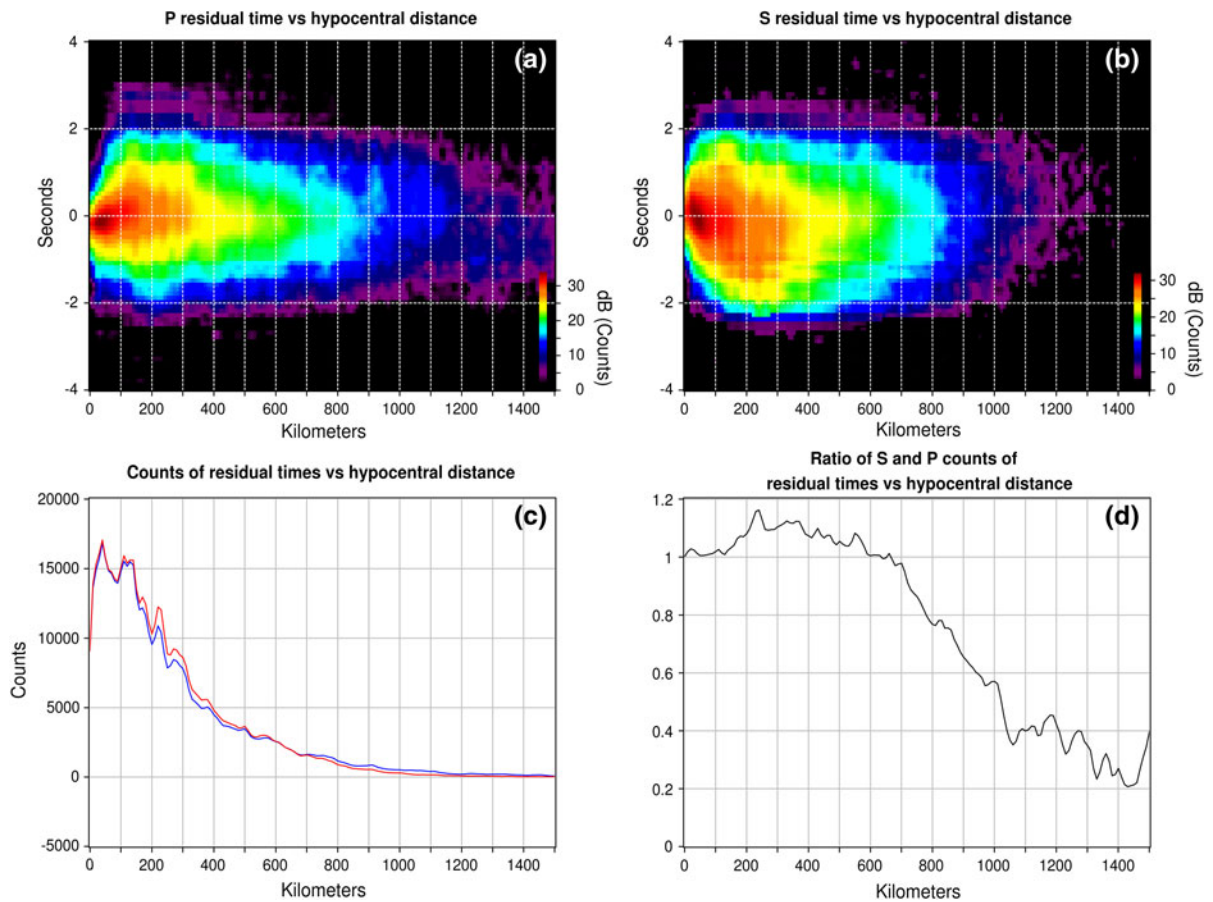


Figure 3

a *P* residual times (in seconds, counts in dB) versus hypocentral distance (in km). **b** *S* residual times. In both cases clusters of 0.1 s for residual time and 10 km for hypocentral distance were taken. **c** Counts of *P* (blue color) and *S* (red color) residual times. **d** Variation of the *S/P* ratio with hypocentral distance

volcanic eruptions. The high noise level detected is probably a direct consequence of the geological structure and particular geodynamics of the islands themselves. In fact, the seismic stations are generally characterized by high-level noise (McCREERY *et al.*, 1993). Furthermore, the persistent volcanic–seismic activity with frequent volcanic tremors makes this zone the noisiest area of Spain.

4. Residual Travel Times and Variances

As is well known, an earthquake is identified (located) on the basis of its hypocentral properties, which are its origin time T_0 and position (x_0, y_0, z_0) and the associated uncertainties $(\sigma_T, \sigma_x, \sigma_y, \sigma_z)$. These

values are determined by inversion of the arrival times of the seismic phases read on seismograms recorded by the stations that make up the surveillance seismic network. Estimation of the focal data is typically performed in an iterative way by minimizing the Euclidean norm of the time residuals, ΔT , i.e., the differences between observed travel times, T_{obs} , and calculated times, T_{cal} :

$$\Delta T = T_{\text{obs}} - T_{\text{cal}} \quad (1)$$

The reading errors can be regarded as random, so statistical analysis of the sign of ΔT on seismic rays propagating across the same domain can provide information about anomalies with average speeds above (+) or below (–) of those of the reference model.

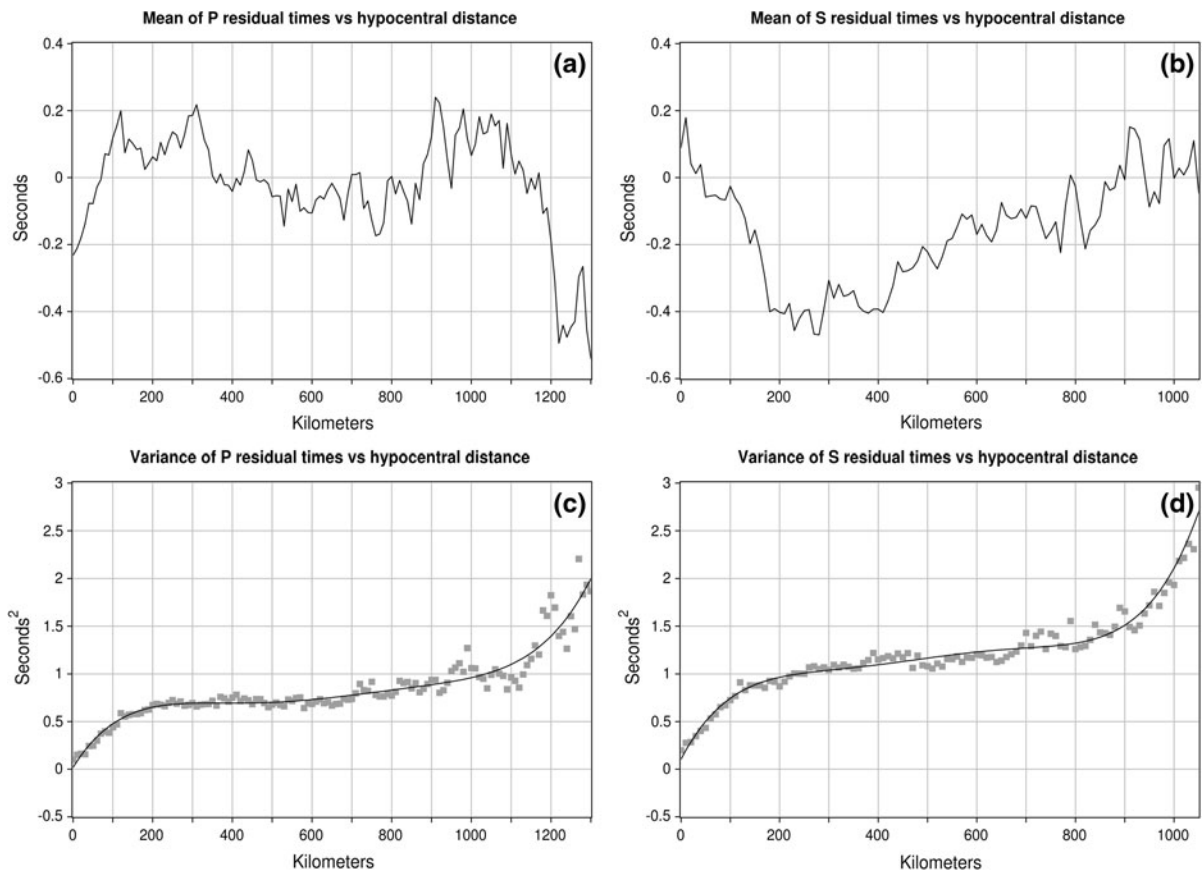


Figure 4

a Mean values of *P* residual times as a function of the hypocentral distance. **b** Mean values of *S* residual times. **c** Variance of *P* residual times versus hypocentral distance and curve fitted by polynomial regression. **d** Variance of *S* residual times and curve of polynomial regression

Assuming the absence of systematic errors because of time readings, the uncertainties in hypocenter location depend mainly on the variance of residual times. The variance of residual time $\sigma_{\Delta T}^2$ is, in turn, a function of the variances of WSR (σ_{WSR}^2) and the velocity uncertainties of the model used for inversion (σ_{MOD}^2). Assuming the statistical independence of σ_{WSR}^2 and σ_{MOD}^2 , we have:

$$\sigma_{\Delta T}^2 = \sigma_{\text{WSR}}^2 + \sigma_{\text{MOD}}^2 \quad (2)$$

For WSR values greater than 10 in the 0.1–10 Hz frequency range, σ_{WSR}^2 , related to the time reading of the Pg and Pn seismic phases, is very small and takes values close to 0.01 s² (ZEILER and VELASCO, 2009). However, it has been experimentally observed that the variance of residual time $\sigma_{\Delta T}^2$ takes much larger values and this difference is attributed to the second term of Eq. (2). Therefore, the variance σ_{MOD}^2

introduced by use of an inadequate velocity model that fails to account for the geological complexity of the monitored area can take values much higher than the uncertainty of the selected data. Large values of σ_{MOD}^2 indicate that the model fails to adequately account for the velocity structure of the monitored region. $\sigma_{\Delta T}^2$ can be attributed to a deficient choice of the velocity model used routinely for hypocenter location, but also to anisotropy of the medium (ROTHMAN *et al.*, 1974).

Experimental separation of the two terms in Eq. (2) is difficult. In this work we estimated an empirical law that binds the variance of residual time to the hypocentral distance. To this end, we considered the one-dimensional *P* wave velocity model used by the IGN (discussed in section “Power Spectral Density Curves of Ground Acceleration”) together with the *S* velocity model obtained by

dividing by 1.73 (Poisson's ratio is 0.25). P and S seismic phases generated by earthquakes located by the SNSN between 1990 and 2010 were used to create two different databases of residual times versus hypocentral distance. We used databases consisting of more than one million residual time–hypocentral distance pairs to construct the histograms represented in Fig. 3. Clusters of 0.1 s for residual time and 10 km for hypocentral distance were considered with this purpose. For each distance we calculated the variance of residual times up to the maximum hypocentral distance of 1,300 km for P phases and 1,050 km for S phases, because lack of data makes the statistical estimates insignificant beyond these values. Figure 3a, b shows histograms of P and S residual times on a logarithmic scale as respective functions of the hypocentral distance. The histogram of P residual times is almost symmetrical in shape whereas the histogram of S residual times has a slight tendency toward negative values. Both histograms, however, show spreading of about ± 2 s, which can be modeled as the sum of random scatter in the measured times because of reading errors and systematic travel time differences caused by lateral heterogeneity.

Figure 3 also shows counts of P and S residual times (Fig. 3c) and from here the variation of the S/P ratio (Fig. 3d), in both cases versus hypocentral distance. As can be seen, the two types of counts of P and S residual times have very similar shapes with a common local maximum at approximately 40 km, a value from which both functions gradually decrease with distance. The S/P ratio is approximately 1.0 for short hypocentral distance (<200 km), takes values greater than 1.1 for intermediate distance (200–550 km) and is smaller than 1.0 for large distance (>600 km), and falls below 0.4 for hypocentral distance larger than 1,000 km. Therefore, up to hypocentral distances of 500–600 km the S phases contribute significantly to hypocenter location. At each station the use of seismic phases with different transmission speeds has the effect of constraining the hypocenter location better, which is generally advantageous when using multiple phases at each seismic station whenever these phases are correctly identified. As the statistical analysis of seismic phases from earthquakes catalogued by the IGN for

the years 1990–2010 shows a Sg/Pg ratio equal to 1.20 and a Sn/Pn ratio equal to 0.82, we conclude that both Sg and Sn phases contribute significantly to the hypocentral location process.

Mean P and S residual times as a function of the hypocentral distance are shown in Fig. 4a, b. The P residual times vary between -0.2 and 0.2 s up to hypocentral distance of 1,200 km; these times initially take small negative values and then small positive values at short distances (up to approximately 500 km), and again negative values from 500 to 900 km; from 900 to 1,200 km the curve of mean values is over zero and beyond 1,200 km falls drastically below zero. Instead, the S residual times take negative values for almost all the hypocentral distances and especially from 200 to 400 km where they reach -0.4 s. This behavior is probably related to the velocity model used for location. Clearly, the S velocity model gives acceptable values of average residual times at short (<100 km) and large (>600 km) distances, but is too fast for intermediate distances. Because non-zero mean values of residual times may introduce systematic location errors, the P velocity model and, especially, the S velocity model used for earthquake location must be optimized or upgraded.

Figure 4c, d also shows the variance of P and S residual times as a function of the hypocentral distance. These variances can be adjusted by polynomial fitting. The choice of polynomial degree is critical for good predictability of the solution, so we used statistical criteria. When the polynomial degree increases the solution is closer to the observed data, but also to random errors. The way in which the solution behaves can be studied through the bias and variance: bias quantifies the deviation from the average estimate of the optimum estimator and variance quantifies the stability of the estimator relative to the observed data. In general, when the complexity increases, the bias decreases whereas the variance increases. To properly balance these two quantities for optimum modeling, we determined the expected prediction error and from here the degree of the polynomial that minimizes this error. The fifth-order polynomials obtained by regression from the variance of P and S residual times are:

$$\begin{aligned}\sigma_p^2 = & 1.065 \times 10^{-14}x^5 - 3.461 \times 10^{-11}x^4 + 4.297 \\ & \times 10^{-8}x^3 - 2.470 \times 10^{-5}x^2 + 6.626 \times 10^{-3}x \\ & + 1.981 \times 10^{-2}\end{aligned}\quad (3)$$

$$\begin{aligned}\sigma_s^2 = & 4.043 \times 10^{-14}x^5 - 1.010 \times 10^{-10}x^4 \\ & + 9.596 \times 10^{-8}x^3 - 4.324 \times 10^{-5}x^2 + 9.846 \\ & \times 10^{-3}x + 1.039 \times 10^{-1}\end{aligned}\quad (4)$$

These expressions describe σ_p^2 and σ_s^2 varying with hypocentral distance (x); they can be interpreted in terms of σ_{MOD}^2 and are valid for hypocentral distances up to 1,300 km for P times and 1,000 km for S times.

Both σ_p^2 and σ_s^2 have a similar behavior and increase rapidly as the hypocentral distance increases. In effect, σ_p^2 and σ_s^2 have an almost linear upward trend at hypocentral distances of less than ca 200 km. Within this interval the first energy arrivals correspond to phases that have propagated mainly across the crust; such a trend would be justified by the complex seismic velocity structure and the heterogeneity of the Iberian crust. For hypocentral distances between approximately 200 and 800 km, both σ_p^2 and σ_s^2 tend to stabilize at approximately 0.75 s^2 for P waves and approximately 1.25 for S waves. In this interval the first energy arrivals are seismic phases that have traveled primarily across the upper mantle, so the behavior of the variances is therefore attributable to the greater homogeneity of the upper mantle compared with the crust. Instead, for hypocentral distances larger than 800–900 km both variances begin to grow rapidly. This behavior is because of the inadequacy of the 1D velocity model at deeper depths when used by the IGN for earthquake location.

Equations (3) and (4) can be used to numerically estimate the variance of P and S residual times at each station. The uncertainties in the readings are given by the covariance matrix C_d , whose diagonal elements are the variances of the residual times at particular stations; the off-diagonal elements are the covariances that describe the errors for pairs of stations. Under the reasonable assumption that there is no correlation between reading errors of arrival times at different stations, we set the off-diagonal elements of C_d equal to zero.

5. Power Spectral Density Curves of Ground Acceleration

The Fourier spectrum of the impulse produced by the source function $S(t)$ is a complex function $S(\omega)$ that is tied to a specific directivity function. This is a direct consequence of the finite nature of the source and implies a variation of the spectrum relative to the direction of observation. In fact, because of destructive interferences of the seismic waves emitted by the source, some frequencies cannot be observed and the high frequencies are attenuated according to power laws of the type $\omega^{-\gamma}$. For these reasons, $S(\omega)$ is often replaced by its envelope $\bar{S}(\omega)$ and plotted in a log–log plot. The near-field and far-field approaches describing the seismic spectrum are well known for different models of earthquakes. Because the experimental observations are generally made at hypocentral distances that are much greater than the average size of the seismic source, the far-field approach is more frequently used.

The waveform coming from the source may change substantially during its propagation both in amplitude and in frequency content. Thus, the spectrum $\bar{S}(\omega, x)$ of the seismic signal at the generic receiver R at position X is expressed in the form:

$$\bar{S}_R(\omega, x) = \bar{S}(\omega)E(x)A(\omega, x) \quad (5)$$

Here $E(X)$ represents the attenuation effects in a perfect elastic medium, namely: geometrical spreading of the wavefront $G(x)$, energy partition at buried interfaces $P(x)$ and free surface effects $F(x)$; $A(\omega, x)$ accounts for energy dissipation due to imperfect elasticity and scattering. Consequently:

$$E(x) = G(x)P(x)F(x) \quad (6)$$

The imperfect elasticity of rocks and the presence of small-scale heterogeneity cause frequency-dependent attenuation of the wavefield $A(\omega, x)$ that can be expressed as

$$A(\omega, x) = I(\omega, x)S(\omega, x)B(\omega) \quad (7)$$

where $I(\omega, x)$ represents the attenuation that depends on the rheology of the medium, $S(\omega, x)$ the attenuation due to scattering, and $B(\omega)$ the transfer function of the top soil layers beneath the station.

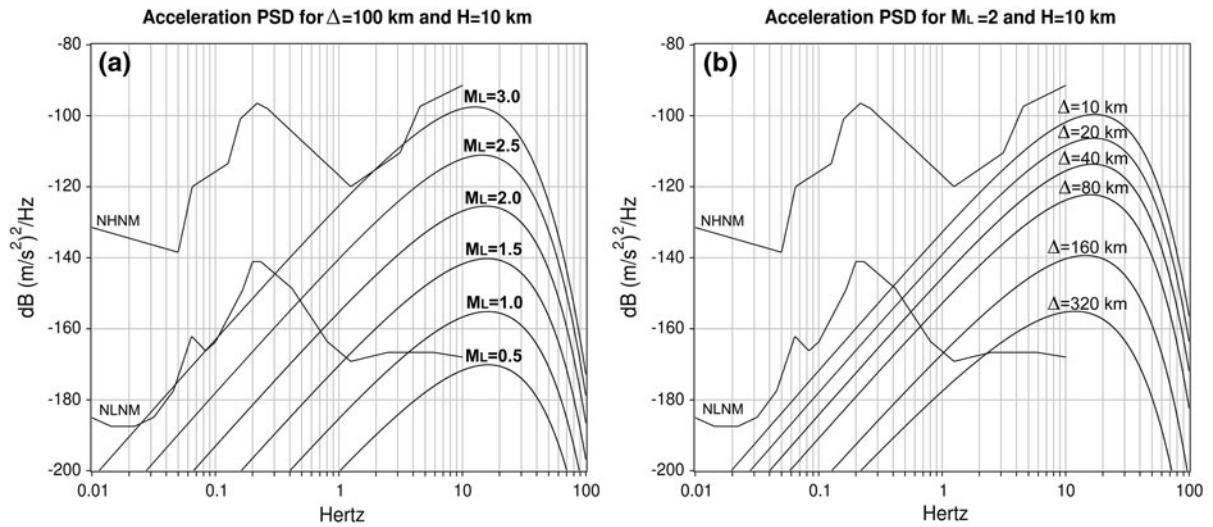


Figure 5

PSD curves (in dB) obtained from noise records: **a** epicenter distance $\Delta = 100$ km and M_L magnitude varying between 0.5 and 3.0; **b** M_L magnitude 2.0 and epicenter distance Δ varying between 10 and 320 km. In both cases the focal depth was fixed at 10 km. The NHNM and NLNM spectra derived from the vertical component of the ambient noise by PETERSON (1993) were also plotted for comparison

Equations (5), (6), and (7) and a seismic source model were used to compute power spectral density curves. For earthquakes of small-to-intermediate magnitude the length (L) and width (W) of the rupture fault are comparable ($L \approx W$), and the circular fault model of BRUNE (1970) is appropriate for these events. The values assigned to seismic source variables were: $\alpha = 6.1$ km (P wave velocity in the medium), $\Delta\sigma = 6$ MPa (stress drop), $R_p = 0.55$ (mean square value of the directivity function for P wave), $V_C = 0.9\beta$ (rupture velocity as fraction of the shear velocity in the medium), $k = 3.36$ (constant that depends on the velocity of the fault rupture and the time of released stress), and $\delta = 0.035$ s⁻¹ (ANDERSON and HOUGH, 1984; GARCÍA-GARCÍA *et al.*, 1996). The frequency-dependent attenuation was modeled by the law $Q_\beta = 100f^{0.7}$ (BURDICK, 1978; PAYO *et al.*, 1990; AKINCI *et al.*, 1995; GARCÍA-GARCÍA *et al.*, 1996; PUJADES *et al.*, 1997) taking into account the ratio $Q_\alpha/Q_\beta = 1.5$ between quality factors (SATO *et al.*, 2002). Specific details about computation algorithms can be found in D'ALESSANDRO *et al.* (2011a).

The focal depth for numerical simulation was fixed at 10 km, being to the most frequently observed depth of Iberian earthquakes (BADAL *et al.*, 2005b). As reference we took the one-dimensional P wave

velocity model used normally for earthquake location by the IGN, which is different from the model used by RUEDA and MÉZCUA (2005) for near-real-time seismic moment–tensor determination in Spain. It consists of three homogeneous flat elastic layers of thickness 11, 13, and 7 km, and velocity 6.1, 6.4, and 6.9 km/s, respectively, on a half-space with a P velocity of 8.0 km/s. The S velocity model was obtained by dividing P velocity by 1.75 (Poisson's ratio is 0.25). The values of crustal density and S wave velocity used in the calculation were estimated from the empirical relationships between elastic wavespeeds and the density of BROCHER (2005).

The PSD of acceleration was calculated from the seismic source model, the velocity model, and the attenuation law described above, by use of the formula:

$$PSD = 10 \log_{10} \left(\bar{S}_R(\omega, x)^2 \right) \quad (8)$$

Figure 5 shows the PSD curves (in dB) obtained as a function of magnitude and epicenter distance. The left plot corresponds to an epicenter distance of 100 km, focal depth $H = 10$ km, and M_L magnitude ranging from 0.5 to 3.0; in contrast, the right plot corresponds to M_L magnitude 2.0, same focal depth,

and epicenter distance ranging from 10 to 320 km. The NHHM and NLNM spectra derived from the vertical component of the ambient noise by PETERSON (1993) were also plotted for comparison. Both plots clearly illustrate that the PSD curves depend on magnitude and epicenter distance, but in all cases their maximum values are found at approximately 10–12 Hz.

6. Estimation of Hypocentral Variables

6.1. Implementation

The seismic wave travel times at stations are nonlinear functions of the focal variables (origin time and source coordinates) and the velocity model being used. The problem can be linearized by using a Taylor series expansion (truncated at the first term) around approximate values of the focal variables sufficiently near the real ones; then, for i -station, it is possible to write:

$$t_i = t'_i + dt_i + (\partial t_i / \partial x) dx + (\partial t_i / \partial y) dy + (\partial t_i / \partial z) dz, \quad i = 1, 2, \dots, N \quad (9)$$

where t'_i is the theoretical time at i -station calculated from an initial solution and $\partial t_i / \partial x$, $\partial t_i / \partial y$, and $\partial t_i / \partial z$ are the partial derivatives of the travel time with respect to the source data (x , y , z). The forward problem can be expressed in the compact form:

$$d = G m \quad (10)$$

where d is the N -dimensional vector of travel time data, m is a four-dimensional vector (dt_i , dx , dy , dz)^T containing the small perturbations or unknowns, and $G = [1, \partial t_i / \partial x, \partial t_i / \partial y, \partial t_i / \partial z]$ is the operator of partial derivatives that maps vectors in the model space into vectors in the data space. Solution of this algebraic equation system, $m' = G^s d$, requires calculation of the generalized inverse matrix G^{-s} and minimization of the functional $\|G m' - d\|$ under the L_2 -norm. This inverse matrix has size $N \cdot 4$ and generally $N > 4$ by which the problem is over-determined. Once the inverse matrix G^{-s} is calculated, the classical least-squares solution of the problem is:

$$m = (G^T G)^{-1} G^T d \quad (11)$$

which can be reformulated through the Lanczos singular-value decomposition to obtain the damped least-squares solution together with the resolution and covariance matrices. Because C_d is the data covariance matrix (discussed in the section “Residual Travel Times and Variances”), the model covariance matrix is:

$$C_S = G^{-s} C_d [G^{-s}]^T \quad (12)$$

which provides the uncertainties in the results: origin time T_0 and hypocenter coordinates (x_0 , y_0 , z_0).

The uncertainty in the determination of any hypocentral variable with a confidence interval of 95 % can be estimated through the χ^2 -distribution with four degrees of freedom. Thus, the uncertainty r_{par} in the value of a generic focal variable is given by:

$$r_{\text{par}} = \sqrt{9.488 \cdot \sigma_{\text{par}}^2} \quad (13)$$

where σ_{par}^2 is the variance of the focal variable and 9.488 is the value of $\Delta\chi^2$ for the confidence level 95 %. The axes of the ellipsoid of confidence were obtained by removing the terms related to time origin in C_S and then performed a canonical representation. To estimate an average error of location, we proceed to compute the radius of the equivalent sphere (RES) defined as:

$$\text{RES} = \sqrt[3]{r_1 \cdot r_2 \cdot r_3} \quad (14)$$

where r_1 , r_2 and r_3 are the semiaxes of the ellipsoid. It is important to point out that this type of error contains no bias in location introduced by systematic errors, so the real error will usually exceed this estimate.

6.2. SNES Maps

We investigated the performance of the SNSN in its current configuration, for trial M_L magnitudes 2.0, 2.5, and 3.0 and focal depth 10 km. After trying different grid-sizes to ensure the consistency of the results, we discretized the study area using a regular mesh having sides of 5 km, then simulated seismic rays propagating from virtual seismic sources placed

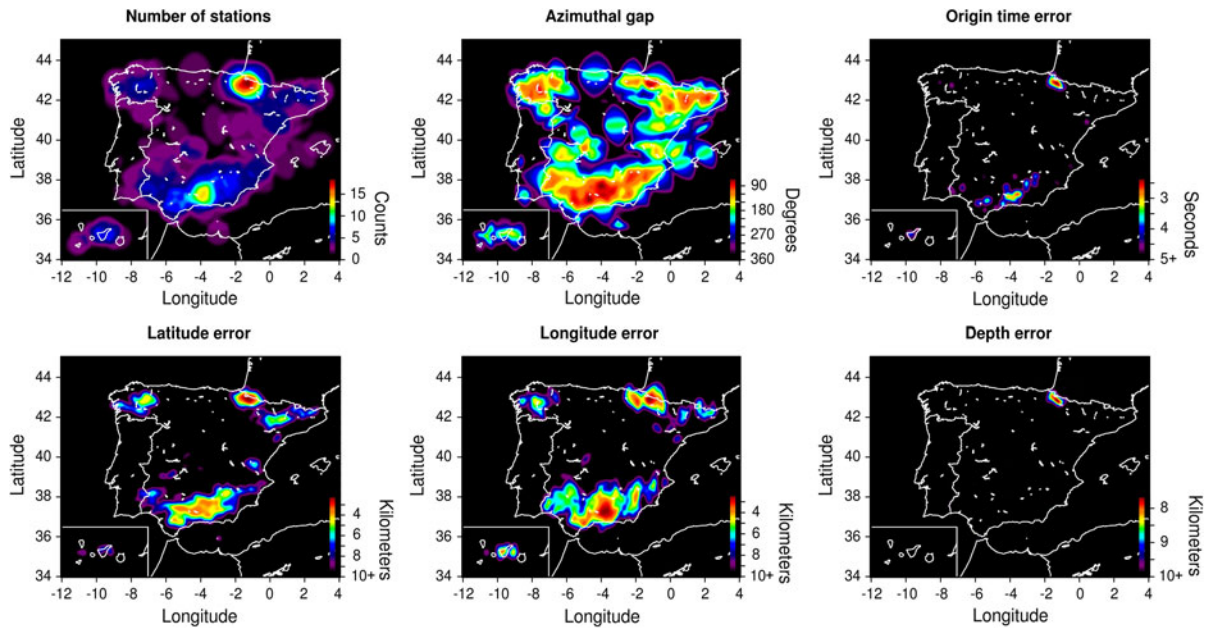


Figure 6

Maps for M_L magnitude 2.0, hypocentral depth 10 km, and confidence level 95 %. For this magnitude, the number of recording stations was 18 and the azimuthal gap did not decrease below 75° . Only three small areas seem to be well covered for epicenter estimation with expected errors of 5 km or less. The hypocentral depth of shallow earthquakes is well constrained within a small area to the north

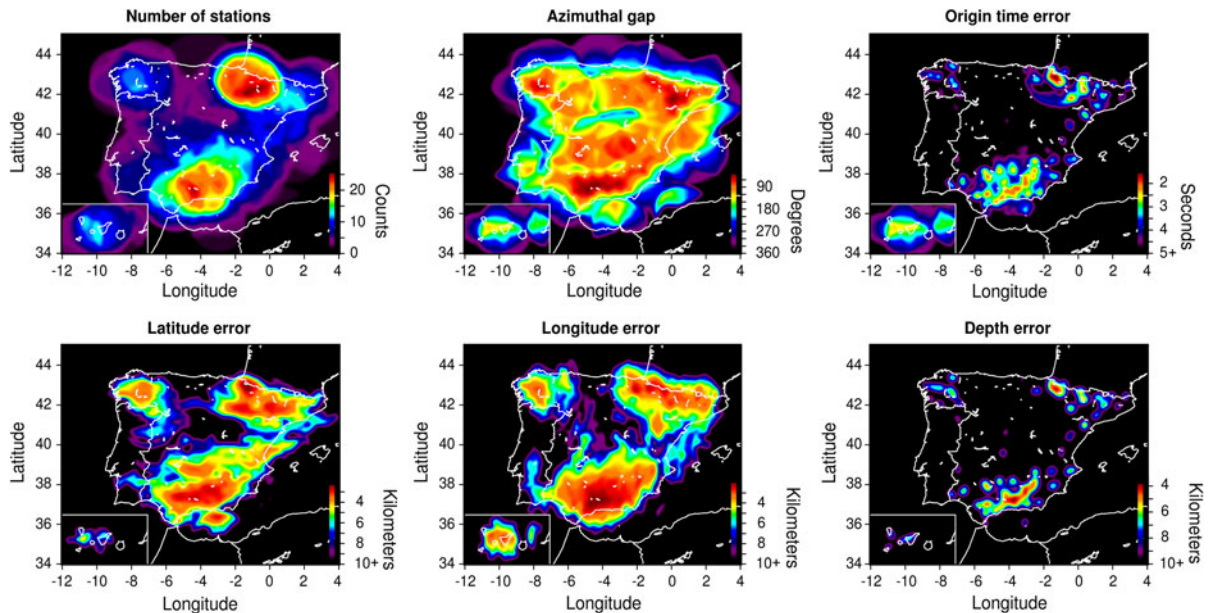


Figure 7

Maps for M_L magnitude 2.5, hypocentral depth 10 km, and confidence level 95 %. Now the number of recording stations is increased up to 25 and the azimuthal gap did not decrease further. With the exception of a few zones in central Spain, most of the territory seems to be well covered for epicenter determinations with expected errors of approximately 4 km or less. A minimum can be observed to the south. Nevertheless, except for two small areas, the rest reflects hypocentral depth estimates with errors that are never below ca. 4 km

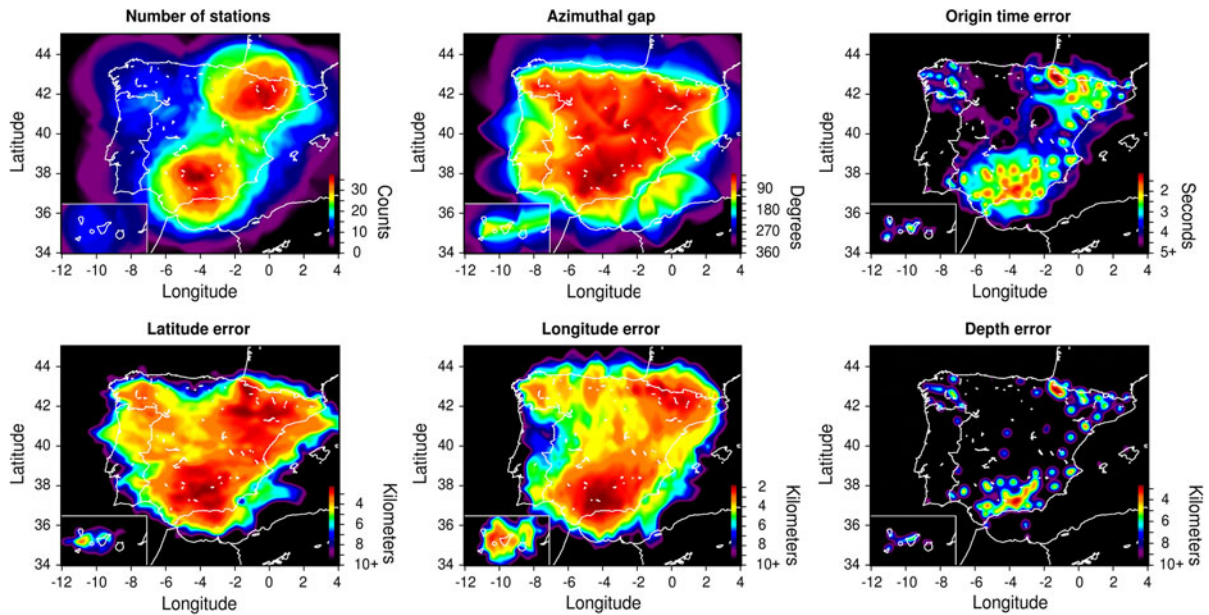


Figure 8

Maps for M_L magnitude 3.0, hypocentral depth 10 km, and confidence level 95 %. For this magnitude, the maximum number of recording stations is above 35 and the minimum azimuthal gap drops to approximately 30° . Almost the whole Spanish territory and part of Portugal appear well covered for epicenter estimation with minimum errors to the north and south. Although epicenter errors reach 2–3 km over almost the whole area monitored by the SNSN, the errors in hypocentral depth continue to be relatively high and seem to be below 4 km in some small areas only

at the grid nodes. We applied the SNES method by ray tracing as a way of mapping hypocentral variable estimates within the confidence interval 95 %. For each station we computed the power spectrum PSD_S on the vertical acceleration record of the noise and then calculated the wideband spectral ratio WSR in the typical 1–12 Hz typical frequency range of the seismic phases generated by regional events:

$$WSR_{(1-12\text{Hz})} = 10 \log_{10} \left(\frac{\int_1^{12} PSD_E df}{\int_1^{12} PSD_S df} \right) \quad (15)$$

where PSD_E is the power spectrum of the synthetic P -signal. Stations with $WSR > 10$ were declared “active” for location of the simulated event. After identifying all active stations for P motion, S motion was considered only at those stations with high WSR and, in any case, by keeping the average P phase number/ S phase number ratio established in the seismic catalog of the IGN.

Figures 6, 7, and 8 show three sets of SNES maps drawn for M_L magnitudes 2.0, 2.5, and 3.0, respectively (here we make reference to local magnitude,

although the earthquake catalog of Spain edited by the IGN does not use M_L , but rather m_{bLg} , m_b , or M_w , and most of the regional earthquakes are sorted by m_{bLg}). In turn, each of these sets is composed of six different SNES maps that report the number of active stations and azimuthal gaps, and also uncertainties in origin time, latitude and longitude, and hypocentral depth. The azimuthal gap is a value often used to provide an indication of the reliability of the epicenter solution; it is defined as the maximum azimuthal gap to the epicenter between two successive stations. An azimuthal gap of 180° or larger indicates that all the stations are on one side of the event. As before, during the mapping process we performed 2D smoothing using a moving square window having sides of five points followed by cubic spline interpolation for reduction of possible local effects and to improve the appearance of the maps.

Events with M_L 2.0 (Fig. 6), seem to be recorded by at least 13–15 stations in the westernmost end of the Pyrenean band and much of the Betics (Fig. 1b); these are, therefore, the peninsular zones best-covered by the SNSN. The azimuthal gap is not less

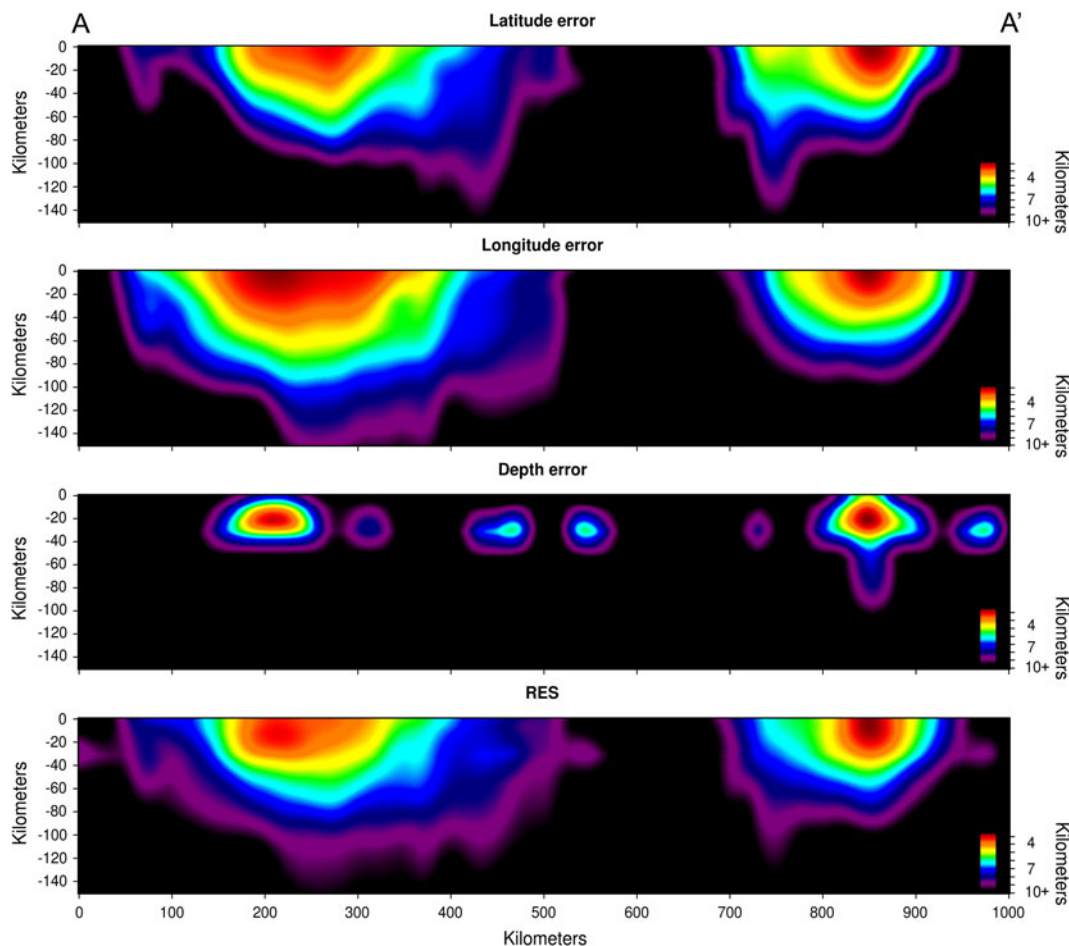


Figure 9

Vertical section along the transect AA' in north–south direction (Fig. 1b) indicating how the error in hypocentral location and RES error vary both laterally and with depth (down to 140 km). The mapping was performed for M_L magnitude 2.5 and confidence level 95 %. For this magnitude the epicenter seems to be well constrained up to a depth of 60 km, and a similar pattern can be seen for RES error, whereas the hypocenter location seems constrained only down to 40 km beneath the areas with the highest station density. A minimum value of the error in hypocentral depth of approximately 3 km is clear at a depth of 20 km. The spatial gap at offset from 550 to 700 km is simply because of the very low density of stations in northern and central Spain

than 75° . For this magnitude, expected epicenter errors reach 4 km or less, and the focal depth of shallow earthquakes is hardly constrained.

For M_L 2.5 (Fig. 7) the maximum number of active stations increases to 25; the azimuthal gap does not decrease further, however. The error in origin time is approximately 2 s in the areas named above and the uncertainty in focal depth reaches 4 km or slightly more. With the exception of a few areas in the central part and in the north of the peninsula, most of the Spanish territory is well covered for epicenter estimation with expected errors of approximately 4 km or less.

For M_L 3.0 (Fig. 8) the maximum number of active stations exceeds 35 and the azimuthal gap drops to approximately 30° . For this magnitude almost the whole of the Iberian territory (Canary Islands included) appears well covered for epicenter location, the error being of the order of 2 km. In particular, both the Pyrenees and the Betic Cordillera (south Spain), the two most seismically active regions of Iberia, and to a lesser extent the east of the peninsula, seem to be well monitored. However, origin time and depth—this last variable is by far the most difficult to obtain precisely in regional events—are not yet satisfactorily constrained.

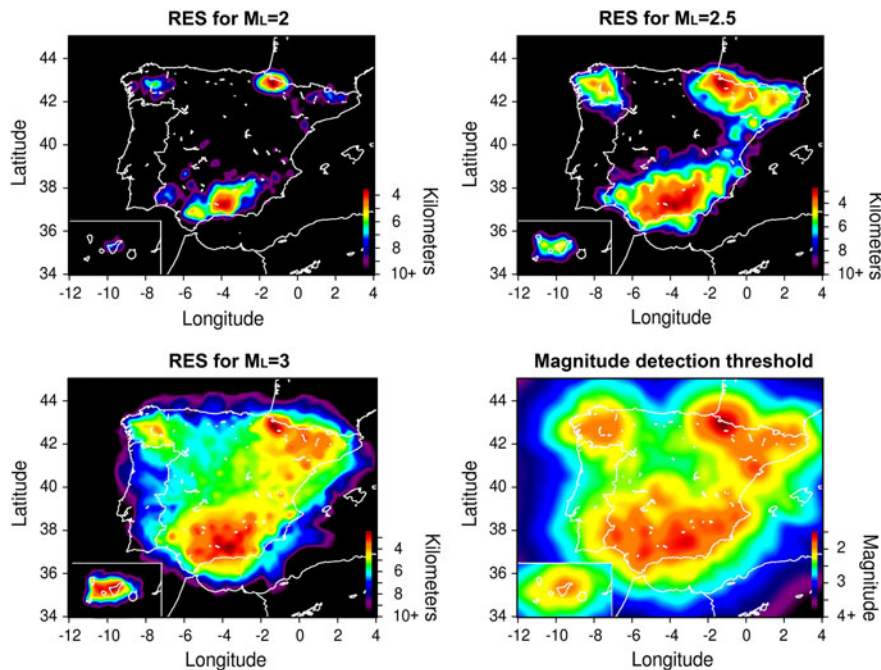


Figure 10

Mapping of the average error in hypocentral location obtained through the radius of the equivalent sphere (RES error) for M_L magnitudes 2.0, 2.5, and 3.0. These maps, which define the uncertainty in the position of the earthquake hypocenter, are based on the semiaxes of the error ellipsoid calculated with a confidence level 95 %. The magnitude detection threshold is defined as the magnitude of the smallest seismic event detected by at least four network stations (*bottom right corner*)

From analysis of SNES maps we observe that an increase in magnitude results in an increase in the area covered by the SNSN and greater accuracy of location of the epicenter. In general, for $M_L > 2.5$ the Spanish territory, Canary Islands included, is well covered for accurate determination of epicenters but not for depth estimation. This is because the derivative of travel time with respect to the depth varies slowly with depth unless the station is near the epicenter. In other words, the depth can be moved up and down without it having much effects on travel time. The focal depth is, however, well constrained when the seismic phases involved in hypocentral location lead to a different sign of the partial derivatives, such as happens for up-going Pg and down-going Pn phases observed very locally and when there is an high S/P ratio, i.e. when a high density of stations is near the epicenter.

6.3. A Glance at Depth Section

With the intention of imaging the results from earthquake location more clearly, we show in Fig. 9a

vertical section along a north–south profile from point A (35.41°N , -4.64°E) to point A' (43.94°N , -0.85°E), crossing the western end of the Pyrenean range, the Ebro Basin, the Iberian Cordillera, the Tagus Basin, the Betic Cordillera and finally the westernmost part of the Alboran Sea (Fig. 1b). The Duero Basin and the Iberian Massif remain on the left of the profile. In the illustration, the three upper panels show uncertainties in source location for M_L magnitude 2.5 with confidence level 95 %; the average error defined by the radius of the equivalent sphere is mapped in the lower panel. The four cross-sections, which have very similar patterns both laterally and with depth, represent the errors affecting the reference data. As can be seen, except for distances between 550 and 700 km where there is a gap because of the very low density of stations over the northern third and center of the Iberian Peninsula (Fig. 1d), the seismic source seems well constrained along much of the profile, in particular along two transects that are the northern half of the profile and the Betic Cordillera and Alboran Sea (Fig. 1b). Errors in epicenter latitude

and longitude are very small for near-surface earthquakes, increasing gradually as the depth increases, but remaining under 5 km even at depths of 60 km.

The error in focal depth reaches a minimum value of 3 km at 20 km depth. The hypocentral depth seems to be well constrained down to 35–40 km beneath the zones with the highest density of stations (Fig. 1d), with error less than 5 km. Deep earthquakes involve almost vertical seismic rays by which they are able to constrain the focal depth; they also involve greater variances of residual times, however. So, the minimum error in hypocentral depth would be probably a trade-off between these two effects.

6.4. RES Maps

To evaluate the seismic hazard in the Ibero-Maghrebian area, PELÁEZ MONTILLA and LÓPEZ CASADO (2002) identified several seismogenic areas over the entire Iberian Peninsula by the presence of seismic sources causing shallow seismicity (uppermost 30 km). One way of assessing the extent to which these areas are well monitored by the SNSN when locating a seismic source consists in determining the average error from the semiaxes of the ellipsoid of confidence and calculating the radius of the equivalent sphere (RES). Figure 10 shows RES maps of uncertainty in the hypocenter computed for M_L magnitudes 2.0, 2.5, and 3.0, focal depth $H = 10$ km, and confidence level 95 %.

The map for $M_L 2.5$ reveals that the station density in the northwestern quadrant of the peninsula and in the two Iberian areas with more highlighted seismicity and seismic hazard, the Pyrenees and the Betic Cordillera (Fig. 1a,c), enables determination of the focus of an earthquake with an error of approximate 3 km. For $M_L 3.0$ much of the peninsula and Canary Islands seem to be monitored to achieve an accuracy in focal location of ca 4 km, and even 3 km in many parts of the aforementioned seismogenic areas.

The seismogenic zone to the northwest of the peninsula contains active faults that are the origin of small and frequent earthquakes. The RES maps enable to say that this area, although having low seismic activity, is acceptably monitored for $M_L \geq 2.5$ because the error in earthquake location is approximately 4 km.

The western sector of the Pyrenean mountain range is probably the area best-covered by the SNSN. The high density of seismic stations and the low ambient noise in the zone enable shallow earthquakes even with $M_L \leq 2.5$ to be constrained. For $M_L \geq 2.5$ the whole Pyrenean area is well monitored, with the expected location error being less than 4 km.

The zone of the Betics (south Spain), affected by intense faulting originating in the Betic–Rif complex, is likewise well covered for earthquakes with M_L magnitudes ≥ 2.0 , because the RES error is approximately 4 km and maybe even less. For M_L magnitudes 2.5 and 3.0 the error in hypocenter estimation decreases to approximately 3 km.

The Canary Islands as a whole have a moderate seismic hazard, although Tenerife Island has a maximum offshore because of a seismogenic source potentially capable of generating relatively large-magnitude tectonic earthquakes (GONZÁLEZ DE VALLEJO *et al.*, 2006). This island is comparatively well monitored for $M_L \geq 2.5$; for $M_L 3.0$ the RES error in earthquake location is 3 km.

6.5. Detection Capability of the SNSN

Unlike other estimates (CARREÑO *et al.*, 2003), the magnitude detection threshold is defined here, as noted earlier, as the magnitude of the smallest earthquake recorded at least by four network stations. Therefore, this value does not take into account the uncertainties in the hypocentral variables, which depend on the geometry, density, and noise of the stations that make up the seismic network, and the velocity model adopted. The magnitude detection threshold map, plotted in Fig. 10 (bottom right corner), was obtained in accordance with this criterion. The results demonstrate a detection threshold ~ 2.0 everywhere and rather ~ 1.0 for most of the Iberian Peninsula, especially for the Pyrenees and southern third of the peninsula, coinciding with the most seismically active and best-monitored regions. A local minimum of ~ 1.0 is observed in the westernmost end of the Pyrenees and a value of 2.5 in the center-north of peninsular Spain.

The detection threshold seems to be significantly overestimated in some zones by the coverage level of the SNSN. The Spanish coastal areas provide a clear

example of overestimated coverage. So, the map in Fig. 10 shows good coverage offshore, and the RES map for M_L magnitude 3.0 (Fig. 8) highlights remarkable location errors because of the great azimuthal gap of stations. Another example is supplied by the center-north of the peninsular territory, where we can observe a magnitude detection threshold of approximately 2.5, and the RES map for M_L 3.0 shows relatively high location errors as a consequence of the low density of stations in the zone (Fig. 1d) and the impossibility of constraining the hypocentral depth well.

7. Conclusions

The main purpose of a seismic network is to provide reliable information about earthquakes, especially their focal data and respective uncertainties. From this perspective, the SNES method (D'Alessandro *et al.* 2011a, b, 2012a, b, c) is a useful tool for meeting this requirement. The SNES method, which operates with simulated P and S waves propagating across a velocity–depth elastic model, enables acquisition of first-hand modeling experience to evaluate the capability of a seismic network for hypocentral location and event detection. The method gives the set of stations involved in the earthquake location process and the adequacy of its spatial distribution, and, especially, the error bounds or confidence intervals affecting the solution. In this way, it is possible to obtain well-founded knowledge for planning enlargement and improvement of the network.

The PSD of noise computed in the 1–12 Hz frequency range is a good indicator for assessing the noise level at SNSN stations. Mapping of this variable is very useful for distinguishing areas with high noise level, for example the southern third of the Iberian Peninsula, the Canary Islands, and northern Morocco, from others with less background noise, for example the center and north of peninsular Spain.

Statistical analysis of P and S residual times has enabled us to constrain the variance of these times by means of empirical laws that give its variation with hypocentral distance. This has enabled checking of the suitability of the velocity model used for earthquake location by the IGN. Both the P and

S velocity models can be optimized, especially the latter.

The SNES maps supply valuable information about the real capacity of the SNSN to detect a seismic event, depending on its magnitude and the distribution of stations on national territory, and therefore they are a guide for optimum upgrading of the network with the purpose of monitoring better the different Spanish regions and especially all those seismogenic areas. Given the characteristics of seismicity in Spain, SNES maps were drawn for M_L magnitudes 2.0, 2.5, and 3.0, focal depth 10 km, and confidence level 95 %. The results report on the number of stations involved in the hypocentral location process, how these stations are spatially distributed, and on the focal data and their uncertainties. In general, the events are detected by a sufficient number of unevenly distributed SNSN stations. The geometric configuration of the array might be improved by installation of new onshore (D'Alessandro *et al.*, 2011a) or offshore (D'Alessandro 2009, 2012d) stations to fill the existing gap in the center and north of the peninsula, even though no persistent seismic activity is observed in these zones.

Origin time and focal depth are values that should be better constrained. Nevertheless, most of the national territory is acceptably monitored by the SNSN. In particular, the northwest of the peninsula, the Pyrenees, especially the westernmost segment, the Betic Cordillera, and Tenerife Island are the best-monitored zones.

The RES maps also drawn for M_L magnitudes 2.0, 2.5, and 3.0, focal depth 10 km, and confidence level 95 %, enable estimation of the average error in hypocenter location. The two Iberian areas with low-to-moderate seismicity and comparatively higher seismic hazard, the Pyrenees and the Betic Cordillera, and the northwestern quadrant of the peninsula, are the areas wherein the focus of an earthquake is determined with an approximate error of 3 km. For M_L 3.0 this error is common for almost the whole peninsula and the Canary Islands.

In general, errors in epicenter latitude and longitude are very small for near-surface earthquakes, increasing gradually as the depth increases but remaining under 5 km at depths of 60 km. The error in focal depth reaches a minimum value of 2–3 km at 20 km depth.

Instead, the hypocentral depth seems to be well constrained down to 40 km beneath the zones with the highest density of stations, with error less than 5 km.

The detection threshold of a seismic network indicates simply whether or not the array is able to detect a seismic event of a specific magnitude by a minimum number of stations. Obviously, both the positions of the stations relative to the hypocenter and the errors introduced by the velocity model used in the location routine are not taken into account. For these reasons this value tends to significantly overestimate the performance of the network. Although the detection threshold does not provide any information about the expected error in hypocenter location, it is an indicator of network performance that naturally needs to be complemented by uncertainties in earthquake location and origin time. The map of M_L magnitude detection threshold of the SNSN has a value of approximately 2.5 for most of Spain and still less, almost 1.0, for the western sector of the Pyrenees and the Canary Islands and the southern third of the peninsula.

We have limited ourselves to evaluation of the strengths and weaknesses of the SNSN, which we attribute mainly to the very simple velocity model used for earthquake location and the spatial distribution of the network stations. Beyond the scope of this study, a future task would be revision of the velocity model and the event-detection algorithm to reduce P and S residual times and hypocentral uncertainties, without forgetting improvement of the network geometry (density and clustering of stations).

7.1. Data Sources

The data used in this paper were extracted from the catalogs edited by the Instituto Geográfico Nacional, Madrid (Spain) that are available on the website <http://www.ign.es>.

Acknowledgments

We are grateful to the anonymous reviewer and to the editor Brian Mitchell for their constructive comments and suggestions.

REFERENCES

- AKINCI, A., DEL PEZZO, E. and IBÁÑEZ, J.M. (1995). *Separation of scattering and intrinsic attenuation in southern Spain and western Anatolia (Turkey)*, Geophys. J. Int., 121, 337-353.
- AMORÈSE, D. (2007). *Applying a change-point detection method on frequency-magnitude distributions*, Bull. Seism. Soc. Am., 97, 1742-1749.
- ANDERSON, J.G. and HOUGH, S.E. (1984). *A model for the shape of the Fourier amplitude spectrum of acceleration at high frequencies*, Bull. Seism. Soc. Am., 74(5), 1969-1993.
- BADAL, J., SAMARDJIEVA, E. and PAYO, G. (2000). *Moment magnitudes for early (1923-1961) instrumental Iberian earthquakes*, Bull. Seism. Soc. Am., 90, 1161-1173.
- BADAL, J., DUTTA, U., SERÓN, F. and BISWAS, N. (2004). *Three-dimensional imaging of shear wave velocity in the uppermost 30 m of the soil column in Anchorage, Alaska*, Geophys. J. Int., 158, 983-997.
- BADAL, J., VÁZQUEZ-PRADA, M. and GONZÁLEZ, A. (2005a). *Preliminary quantitative assessment of earthquake casualties and damages*, Natural Hazards, 34, 353-374.
- BADAL, J., VÁZQUEZ-PRADA, M., GONZÁLEZ, A. and ZHANG, Z. (2005b). *Prognostic estimations of seismic risk levels in Spain*, *International Conference 250th Anniversary of the 1755 Lisbon Earthquake*, Lisbon, pp. 198-205.
- BOE (2002). R.D. 997/2002 27-09-2002 on NCSR-02, *Boletín Oficial del Estado* N° 244, pp. 35898-35967 (in Spanish).
- BROCHER T.M. (2005). *Empirical relations between elastic wavepeeds and density in the Earth's crust*, Bull. Seism. Soc. Am., 95(6), 2081-2092.
- BRUNE J.N. (1970). *Tectonic stress and the spectra of seismic shear waves from earthquakes*, J. Geophys. Res., 75, 4997-5009.
- BUFORN, E. and UDIAS, A. (2010). *Azores-Tunisia, a tectonically complex plate boundary*, *Advances in Geophysics*, 52, 3, doi: [10.1016/S0065-2687\(10\)52003-X](https://doi.org/10.1016/S0065-2687(10)52003-X), 1139-1182.
- BURDICK, L.J. (1978). *t^* for waves with a continental ray path*, Bull. Seism. Soc. Am., 68(4), 1013-1030.
- CAO, A.M. and GAO, S.S. (2002). *Temporal variation of seismic b -values beneath northeastern Japan island arc*, Geophys. Res. Lett., 29, no. 9, doi: [10.1029/2001GL013775](https://doi.org/10.1029/2001GL013775).
- CARREÑO, E., LÓPEZ, C., BRAVO, B., EXPÓSITO, P., GURRÍA, E. and GARCÍA, O. (2003). *Seismicity of the Iberian Peninsula in the instrumental period 1985-2002*, *Física de la Tierra*, 15, 73-91 (in Spanish).
- CHEN, Y., BADAL, J. and HU, J. (2010). *Love and Rayleigh wave tomography of the Qinghai-Tibet Plateau and surrounding areas*, *Pure Appl. Geophys.*, 167(10), 1171-1203, doi: [10.1007/s00024-009-0040-1](https://doi.org/10.1007/s00024-009-0040-1).
- D'ALESSANDRO, A., D'ANNA G. LUZIO D., MANGANO G. (2009). *The INGV's new OBS/H: analysis of the signals recorded at the Marsili submarine volcano*, *Journal of Volcanology and Geothermal Research*, 183, 1-2, 17-29, doi: [10.1016/j.jvolgeores.2009.02.008](https://doi.org/10.1016/j.jvolgeores.2009.02.008).
- D'ALESSANDRO, A., LUZIO, D., D'ANNA, G. and MANGANO, G. (2011a). *Seismic Network Evaluation through Simulation: An application to the Italian National Seismic Network*, Bull. Seism. Soc. Am., 101(3), 1213-1232, doi: [10.1785/0120100066](https://doi.org/10.1785/0120100066).
- D'ALESSANDRO, A., PAPANASTASSIOU, D. and BASKOUTAS, I. (2011b). *Hellenic Unified Seismological Network: an evaluation of its*

- performance through the SNES method, *Geophys. J. Int.*, *185*, 1417-1430, doi:10.1111/j.1365-246X.2011.05018.x.
- D'ALESSANDRO, A. and STICKNEY, M. (2012a). *Montana Seismic Network Performance: an evaluation through the SNES method*, *Bull. Seism. Soc. Am.*, *102* (1), 73-87, Print ISSN: 0037-1106, Online ISSN: 1943-3573, doi:10.1785/0120100234.
- D'ALESSANDRO, A., RUPPERT, N. (2012b). *Evaluation of Location Performance and Magnitude of Completeness of Alaska Regional Seismic Network by SNES Method*, *Bull. Seism. Soc. Am.*, *102*, 5, 2098-2115, doi:10.1785/0120110199.
- D'ALESSANDRO, A., DANET, A., GRECU, B. (2012c). *Location performance and magnitude of completeness of the Romanian National Seismic Network*, *Pure and Applied Geophysics*, doi: 10.1007/s00024-012-0475-7
- D'ALESSANDRO, A., MANGANO, G., D'ANNA, G. (2012d). *Evidence of persistent seismo-volcanic activity at Marsili seamount*, *Annals of Geophysics, Scientific News*, *55*, 2, 2012; ISSN: 2037-416X, doi:10.4401/ag-5515.
- GARCÍA-GARCÍA, J.M., VIDAL, F., ROMACHO, M.D., MARTÍN-MARFIL, J.M., POSADAS, A. and LUZÓN, F. (1996). *Seismic source parameters for microearthquakes of the Granada basin (southern Spain)*, *Tectonophysics*, *261*, 51-66.
- GOMBERG, J. (1991). *Seismicity and detection/location threshold in the southern Great Basin seismic network*, *J. Geophys. Res.*, *96*, 16401-16414.
- GONZÁLEZ DE VALLEJO, L.I., GARCÍA-MAYORDOMO, J. and INSUA, J.M. (2006). *Probabilistic Seismic-Hazard Assessment of the Canary Islands*, *Bull. Seism. Soc. Am.*, *96*(6), 2040-2049.
- HENARES, J., LÓPEZ-CASADO, C., BADAL, J. and PELÁEZ, J.A. (2010). *Seismicity pattern of the Betic Cordillera (southern Spain) derived from the fractal properties of earthquakes and faults*, *Earthq. Sci.*, *23*(4), 309-323, doi:10.1007/s11589-010-0728-4.
- JIMÉNEZ, M.J., GIARDINI, D., GRÜNTAL, G. and SESAME Working Group (2001). *Unified seismic hazard modelling throughout the Mediterranean region*, *Boll. Geof. Teor. Appl.*, *42*, 3-18.
- KVAERNA, T., RINGDAL, F., SCHWEITZER, J., and TAYLOR, L. (2002). *Optimized seismic threshold monitoring—Part 1: regional processing*, *Pure Appl. Geophys.*, *159*(5), 969-987.
- LÓPEZ CASADO, C., MOLINA, S., GINER, S.J., and DELGADO, J.A. (2000). *Magnitude-intensity relationship in the Ibero-Maghrebian region*, *Nat. Hazards*, *22*, 271-297.
- MARSAN, D. (2003). *Triggering of seismicity at short timescales following California earthquakes*, *J. Geophys. Res.*, *108*, B5, 2266.
- MCCREERY, C.S., DUENNEBIER, F.K. and SUTTON, G.H. (1993). *Correlation of deep ocean noise (0.4-20 Hz) with wind, and the Holu spectrum a worldwide constant*, *J. Acoust. Soc. Am.*, *93*, 2639-2648.
- MCCNAMARA, D.E. and BULAND, R.P. (2004). *Ambient Noise Levels in the Continental United States*, *Bull. Seism. Soc. Am.*, *94*, 1517-1527.
- MÉZCUA, J. (1995). *Fundamentals of the seismic network in Spain*. In: MÉZCUA, J. (ed.), *Regional Seismic Networks*, Instituto Geográfico Nacional, Madrid (Spain), Monografía 11, pp. 63-86 (in Spanish).
- MIGNAN, A., WERNER, M.J., WIEMER, S., CHEN, C.C. and WU, Y.M. (2011). *Bayesian estimation of the spatially varying completeness magnitude of earthquake catalogs*, *Bull. Seismol. Soc. Am.*, *101*, doi:10.1785/0120100223.
- MUÑOZ, D. and UDIAS, A. (1987). *Three large historical earthquakes in Southern Spain*. In: MÉZCUA, J. and UDIAS, A. (eds.), *Seismicity, Seismotectonic and Seismic Risk of the Ibero-Maghebian Region*, Instituto Geográfico Nacional, Madrid, Monografía 8, pp. 175-182.
- OGATA, Y., and K. KATSURA (1993). *Analysis of temporal and spatial heterogeneity of magnitude frequency distribution inferred from earthquake catalogs*, *Geophys. J. Int.*, *113*, 727-738.
- PAYO, G., BADAL, J., CANAS, J.A., CORCHETE, V., PUJADES, L. and SERÓN, F.J. (1990). *Seismic attenuation in Iberia using the coda-Q method*, *Geophys. J. Int.*, *103*, 135-145.
- PAYO, G., CANAS, J.A. and BADAL, J. (1994). *Seismic hazard and inelastic attenuation in the Iberian Peninsula*. In: *Proc. U.S.-Spain Workshop on Natural Hazards*, Barcelona, Spain, pp. 312-342.
- PELÁEZ MONTILLA, J.A. and LÓPEZ CASADO, C. (2002). *Seismic hazard estimate in the Iberian Peninsula*, *Pure Appl. Geophys.*, *159*, 2699-2713.
- PETERSON J. (1993). *Observation and Modeling of Background Seismic Noise*, U.S. Geol. Surv. Open-File Rept., Albuquerque, pp. 93-322.
- PUJADES, L.G., UGALDE, A., CANAS, J.A., NAVARRO, M., BADAL, J. and CORCHETE, V. (1997). *Intrinsic and scattering attenuation from observed seismic codas in the Almeria Basin (southeastern Iberian Peninsula)*, *Geophys. J. Int.*, *129*, 281-291.
- RODRÍGUEZ DE LA TORRE, F. (1984). *Los terremotos alicantinos de 1829*, Instituto de Estudios Alicantinos, Alicante, Spain, serie I, número 100 (ISBN 84-505-0425-2) (in Spanish).
- ROTHMAN, R.L., GREENFIELD, R.J. and HARDY, H.H. (1974). *Errors in hypocenter location due to velocity anisotropy*, *Bull. Seism. Soc. Am.*, *64*, 1993-1996.
- RUEDA, J. and MÉZCUA, J. (2005). *Near-real-time seismic moment-tensor determination in Spain*, *Seism. Res. Lett.*, *76*, 455-465.
- RYDELEK, P.A. and SACKS, I.S. (1989). *Testing the completeness of earthquake catalogues and the hypothesis of self-similarity*, *Nature*, *337*, 251-253.
- SAMARDIJEVA, E., GONZALO P. and BADAL, J. (1999). *Magnitude formulae and intensity-magnitude relations for early instrumental earthquakes in the Iberian region*, *Natural Hazards*, *19*, 189-204.
- SATO, H., FEHLER, M. and WU, R. (2002). *Scattering and attenuation of seismic waves in the lithosphere*. In: Lee, Kanamori, Jennings and Kisslinger (eds.), *International Handbook of Earthquake & Seismology, Part A*, ISBN: 0124406521.
- SCHORLEMMER, D. and WOESSNER, J. (2008). *Probability of Detecting an Earthquake*, *Bull. Seism. Soc. Am.*, *98*(5), 2103-2117.
- SERENO, T.J. and BRATT, S.R. (1989). *Seismic detection capability at NORESS and implications for the detection threshold of a hypothetical network in the Soviet Union*, *J. Geophys. Res.*, *94*, no. B8, 10,397-10,414.
- SERÓN, F.J., SABADELL, F.J., BADAL, J. and MARTÍN, J.M. (1999). *Modelling techniques for volumetric reconstruction of Earth structures*, *Phys. Chem. Earth (A)*, *24*, 261-268.
- SHEDLOK, K.M., GIARDINI, D., GRÜNTAL, G., ZHANG, P. (2000). *The GSHAP Global Seismic Hazard Map*, *Seism. Res. Lett.*, *71*, 679-686.
- SHEPARD, D. (1968). *A two-dimensional interpolation function for irregularly-spaced data*, *Proceedings of the 1968 ACM National Conference*, pp. 517-524.
- UDIÁS, A. (1999). *Principles of Seismology*, Cambridge University Press, United Kingdom, 475 pp.
- WIEMER, S. and WYSS, M. (2000). *Minimum magnitude of complete reporting in earthquake catalogs: examples from Alaska, the*

- Western United States, and Japan*, Bull. Seism. Soc. Am., 90, 859-869.
- WOESSNER, J. and WIEMER, S. (2005). *Assessing the quality of earthquake catalogs: Estimating the magnitude of completeness and its uncertainties*, Bull. Seism. Soc. Am., 95(4), 684-698.
- ZEILER, C. and VELASCO, A.A. (2009). *Seismogram Picking Error from Analyst Review (SPEAR): Single-Analyst and Institution Analysis*, Bull. Seism. Soc. Am., 99(5), 2759-2770.

(Received June 12, 2012, revised November 5, 2012, accepted November 10, 2012, Published online December 20, 2012)